Clays and Clay Minerals, Vol. 68, No. 6:632–645, 2020

POLYTYPISM OF CRONSTEDTITE FROM NAGYBÖRZSÖNY, HUNGARY

Jiří Hybler[1]*, Zdeněk Dolníček[2], Jiří Sejkora[2], and Martin Števko[3]

[1]Institute of Physics, Academy of Sciences of the Czech Republic, Na Slovance 2, CZ-182 21 Praha 8, Czech Republic
[2]Department of Mineralogy and Petrology, National Museum, Cirkusová 1740, CZ-193 00 Praha 9, Czech Republic
[3]Earth Science Institute, Slovak Academy of Sciences, Dúbravská cesta 9, SK-840 05 Bratislava, Slovak Republic

Abstract—The present study provides an example of the accurate identification of polytypes of trioctahedral 1:1 layered silicates from single-crystal X-ray diffraction data collected with the aid of a four-circle diffractometer equipped with an area detector. Single crystals of the mineral cronstedtite from the Nagybörzsöny gold ore deposit, northern Hungary, were studied. The chemical composition of some crystals was determined by electron probe microanalysis (EPMA). The precession-like images of the reciprocal space (RS) sections created by the diffractometer software and presented in the study were used to determine the OD (ordered-disordered) subfamilies (Bailey's groups A, B, C, D) and particular polytypes. With one exception, all crystals studied belong to subfamily A. The rare polytype 1*M*, a = 5.51, b = 9.54, c = 7.33 Å, β = 104.5°, space group *Cm* is relatively abundant in this occurrence. Another polytype 3*T*, a = 5.51, c = 21.32 Å, space group $P3_1$ was also found. Both polytypes occur separately or in mixed, mostly 1*M* dominant crystals. Some 1*M* polytype crystals are twinned by order 3 reticular merohedry with a 120° rotation along the $\mathbf{c}_{hex}$ axis as the twin operation. A rare 1*M*+3*T* mixed crystal with 1*M* part twinned also contains a small amount of subfamily C. A possible presence of the most common 1*T* polytype of this subfamily cannot be confirmed because of overlap of the characteristic reflections with those of 3*T*. Several completely disordered crystals produced diffuse streaks instead of discrete characteristic reflections on the RS sections. The EPMA revealed Fe, Si, traces of Mg, Al, S, and Cl. One black crystal originally considered to be cronstedtite was identified as (111) twinned sphalerite. Some crystals of cronstedtite are covered partially by a honey-brown crust or small crystals of siderite.

Keywords—1:1 Layer silicate · 1*M* and 3*T* polytypes · Cronstedtite · Polytypism · Single-crystal X-ray diffraction · Stacking disorder · Twinning

INTRODUCTION

The use of modern single-crystal X-ray diffractometers with area detectors enables detailed and extensive studies of minerals affected by polytypism. Several articles dealing with the layered silicate, cronstedtite, from Pohled (Czech Republic), Nižná Slaná (Slovakia), and Chyňava (Czech Republic) (Hybler et al. 2016, 2017; Hybler and Sejkora 2017) have been published recently. Furthermore, electron diffraction tomography (EDT) and/or 3D electron diffraction are appropriate options for polytype identification of submicroscopic crystals, e.g. in synthetic run products (Pignatelli et al. 2013; Hybler et al. 2018), or separated from meteorites (Pignatelli et al. 2016, 2017, 2018).

Cronstedtite was described first from the Vojtěch Mine in Příbram (now Czech Republic) by Steinmann (1820, 1821), and was named in honor of the Swedish chemist and mineralogist Axel Fredrik Cronstedt (23 December 1722–19 August 1765). Pioneering studies classified cronstedtite as a T–O or 1:1 trioctahedral phyllosilicate of the serpentine-kaolinite group, with a general formula $(Fe^{2+}_{3-x}\ Fe^{3+}_{x})(Si_{2-x}Fe^{3+}_{x})O_5(OH)_4$, where $0 < x < 0.85$ (Steadman and Nuttall 1963, 1964; Steadman 1964; Bailey 1969, 1988). Its octahedral sheet is formed by edge-sharing MA_6 octahedra. Ideally, M = Fe, A = O in corners shared with the tetrahedral sheet, while in corners not shared with the tetrahedral sheet A = OH, or rarely F, Cl, S. The tetrahedral sheet is formed by TO_4 tetrahedra grouped in sextuple rings by sharing basal oxygen atoms at the corners. Both sheets form the 1:1 layer (in fact the structure building layer) by sharing apical O atoms of tetrahedra and corners of octahedra. The neighboring layers are connected via hydrogen bonds, where the OH groups of the octahedral sheet serve as donors and the basal oxygen atoms of the adjacent tetrahedral sheets are acceptors. The stacking of consecutive layers is guided by stacking rules of some of four OD (Order-Disorder) subfamilies – Bailey's groups A, B, C, D (Bailey 1969, 1988).

In cronstedtite, Fe enters not only into the octahedral, but also into tetrahedral positions, where Si^{4+} is partially replaced by Fe^{3+}. Presumably an equivalent amount of Fe^{3+} replaces Fe^{2+} in octahedral positions in order to achieve charge balance. Some other divalent cations such as Mg^{2+} and/or Mn^{2+} can substitute for Fe^{2+} in various amounts in octahedral positions (e.g. Steinmann 1821; Geiger et al. 1983; Hybler and Sejkora 2017). The Mn-rich analogue of cronstedtite was found in South Africa and approved as a new distinct mineral species, guidottiite (Wahle et al. 2010).

Crystal-structure refinements of the following polytypes have been published to date: 1*T* (Hybler et al. 2000), $2H_2$ (Geiger et al. 1983; Hybler et al. 2002), 3*T* (Smrčok et al. 1994), 1*M* (Hybler 2014), and $6T_2$ (Hybler 2016). High-resolution transmission electron microscopy (HRTEM) studies of cronstedtite were published by Kogure et al. (2001, 2002).

The aim of the current study was to carry out a thorough examination of polytypism and chemical variation of cronstedtite from Nagybörzsöny, Hungary, with the aid of

* E-mail address of corresponding author: hybler@fzu.cz
DOI: 10.1007/s42860-020-00102-9

single-crystal X-ray diffraction (XRD) and electron probe microanalysis (EPMA).

OCCURRENCE

The famous Nagybörzsöny ore deposit (known formerly also as Deutsch Pilsen) is situated in northern Hungary (Fig. 1), near the Slovakian border, in the Börzsöny Mountains, ~5 km ENE of the village of Nagybörzsöny, and ~50 km NNW of Budapest. The GPS coordinates of the entrance of the main adit (known as Alsó-Rózsa-Taró) are: 47.9408644°N, 18.8943714°E.

The Börzsöny Mountains are part of the Neogene Intra-Carpathian Volcanic Arc. Two periods of volcanic activity occurred during the Middle Badenian (Korpás and Lang 1993): an early extrusive phase (Lower Unit) was followed by a second phase, characterized by a large stratovolcanic structure (Upper Unit). Only the Lower Unit is affected by hydrothermal processes in its central area. The alteration is represented near the surface by an argillite zone with local Au-bearing polymetallic sulfide mineralization (Cu, Pb, Zn ± Ag) in veins and stockworks. This zone grades laterally and vertically into a propylite zone with massive and disseminated copper mineralization. K/Ar ages of both fresh and hydrothermally altered rocks show a Gaussian distribution, with a maximum between 15 and 14 My and an average age of 15.2±0.8 My. The average age of the Upper Volcanic Unit is 14.2 ±0.9 My. Paleomagnetic data indicate that the total period of volcanic activity was <0.7 My. The estimated duration of the early phase, including the hydrothermal event, is between 0.2 and 0.4 My.

The ore mineralization in the Nagybörzsöny area is hosted in Miocene calc-alkaline volcanic rocks and it forms veins and stockwork in a dacite breccia pipe affected by strong propylitic alteration (Pantó and Mikó 1964; Dobosi and Nagy 1989; Korpás and Lang 1993; Nagy 2002). This deposit has been exploited mainly for gold and silver since the Middle Ages, especially in the 14th and 15th Centuries. The area of the Rózsa hill was explored in detail by drilling in 1989 (Nagy 2002). The mineralization at the Nagybörzsöny deposit is multistage (mesothermal to epithermal) with Cu-Fe-(Au-Mo), Zn-Pb-Cu, Bi-Pb-As-W-(Au-Ag-Te), Zn-Pb-Ag-(Cu-Sb), and Au-Ag assemblages (Szakáll et al. 2012). More than 120 minerals have been described from this locality (Szakáll et al. 2016). Two principal stages of the mineralization were distinguished by Koch and Graselly (1953) and Pantó and Mikó (1964). Pyrrhotite, chalcopyrite, and sphalerite are the main minerals of the first stage. The typical minerals of the second stage are arsenopyrite, pyrite, galena, native bismuth, and bismutinite. They are accompanied by other rare sulfosalts and tellurides such as joséite-A, ikunolite, emplectite, canizzarrite, cosalite, pavonite, gustavite, and lillianite (Szakáll et al. 2012; Zajzon et al. 2014). The Nagybörzsöny deposit is the type locality of pilsenite (Kenngott 1853), jonassonite (Paar et al. 2006), and jaszczakite (Bindi and Paar 2017).

According to Koch and Graselly (1953), small (~1 mm) aggregates of cronstedtite were first found by J. Erdélyi (without reference, not dated) in a piece of ore material collected from the dump of the Alsó-Rózsa-Táró. This sample is no longer available. Another sample found by mineral collector Gábor Koller in the same dump in 2000 was used in the present study, therefore.

EXPERIMENTAL

A small piece of the porous, mostly pyrite and siderite ore material (~18 mm×14 mm×8 mm) contained scarce, isolated, lath-shaped or pyramidal black cronstedtite crystals, typically up to 1.5 mm long, in cavities. Some of them were partially covered by a brown crust or small crystals of siderite. Unlike other occurrences, no veins, druses, or aggregates were observed. The crystals were removed by a needle and glued to glass fibers under the stereomicroscope. Some were cleaved into smaller pieces. Polytypes were identified by single-crystal XRD. Some crystals identified previously were used later for determination of the chemical composition using EPMA. All of the crystals selected from the ore material were consumed by the study.

Single-crystal X-ray Diffraction

The fragments of cronstedtite crystals (34 altogether) were tested using the four-circle (double-wavelength) X-ray diffractometer Gemini A Ultra (Rigaku Oxford Diffraction, Kazimierza Witalisa Szarskiego 3, 54-609 Wrocław, Poland) equipped with an Atlas CCD area detector (Agilent

Fig. 1. Outline map of Hungary showing the location of the Nagybörzsöny deposit

Table 1. Lattice parameters (in Å, degrees, with standard uncertainties in parentheses), subfamilies (Bailey's groups), and polytypes of cronstedtite from Nagybörzsöny, Hungary. Minor polytypes in given samples are shown in parentheses. For most mixed crystals, the lattice parameters of dominant polytypes are given. Disordered crystals are indexed with respect of the unit cell of the subfamily structure of the subfamily A identical to that of the 3*T* polytype. In most mixed crystals, lattice parameters of the dominant polytypes are given

Sample	*a*	*b*	*c*	β	Volume	Group	Polytype(s)	Note
NB1	5.5084(8)		21.308(3)	90	559.92(14)	A	3*T*, (1*M*)	3*T* part, selected for EPMA
NB2	5.5143(12)	9.542(2)	7.3526(17)	104.56(2)	374.43(14)	A	1*M*, (3*T*)	1*M* part
NB3	5.5178(13)		21.316(5)	90	562.0(2)	A	3*T*, (1*M*)	3*T* part, 1*M* twinned by 120° rotation
NB4	5.5051(8)		21.311(3)	90	559.34(14)	A	disordered	Subfamily structure, Fig. 6
NB5	5.5069(9)	9.5386(15)	7.345(2)	104.47(2)	373.57(14)	A	1*M*	Diffuse streaks
NB6	5.5025(13)	9.536(2)	7.3288(16)	104.56(2)	372.21(14)	A	1*M*	Fig. 2
NB7	5.5056(8)	9.5334(12)	7.3359(12)	104.48(1)	372.80(9)	A	1*M*	Twinned by 120° rotation, Fig. 3
NB9	5.5090(14)	9.544(3)	7.340(2)	104.54(3)	373.58(18)	A+C	1*M*, 3*T* (1*T*?)	1*M* part twinned, accessory of the subfamily C, Fig. 5
NB10	5.517(3)		21.354(10)	90	563.0(5)	A	disordered	Subfamily structure, selected for EPMA
NB11	5.5059(6)		21.320(3)	90	559.70(11)	A	disordered	Subfamily structure, selected for EPMA
NB14	5.5103(12)		21.337(5)	90	561.1(2)	A	disordered	Subfamily structure
NB15	5.5113(7)		21.317(3)	90	560.75(13)	A	3*T*, (1*M*)	3*T* part
NB16	5.5121(16)	9.541(2)	7.345(2)	104.50(3)	374.01(18)	A	1*M*	pure 1*M*
NB17	5.5087(8)		21.319(4)	90	560.29(15)	A	3*T*, (1*M*)	3*T* part
NB18	5.5079(7)		21.311(3)	90	559.91(13)	A	3*T*, (1*M*)	3*T* part, 1*M* twinned by 120° rotation
NB19	5.5069(9)		21.321(4)	90	559.95(18)	A	3*T*, (1*M*)	3*T* part, selected for EPMA
NB20	5.5047(11)		21.311(5)	90	559.2(2)	A	3*T*, (1*M*)	3*T* part, 1*M* twinned by 120° rotation
NB21	5.5045(7)		21.320(3)	90	559.44(13)	A	3*T*, (1*M*)	3*T* part, 1*M* twinned by 120° rotation
NB22	5.5046(12)	9.532(2)	7.3350(16)	104.54(2)	372.53(14)	A	3*T* + 1*M*	Dominant 1*M* part, Fig. 4
	5.5036(8)		21.305(4)	90	558.86(15)	A	3*T* + 1*M*	Minor 3*T* part
NB23	5.5083(8)		21.318(3)	90	560.15(14)	A	3*T*, (1*M*)	3*T* part
NB24	5.5118(8)		21.322(3)	90	560.96(14)	A	3*T*	pure 3*T*
NB25	5.5099(8)		21.298(3)	90	559.96(14)	A	3*T*, (1*M*)	3*T* part, 1*M* twinned by 120° rotation
NB26	5.5077(13)		21.297(5)	90	559.5(2)	A	disordered	Subfamily structure
NB27	5.5147(11)		21.331(5)	90	561.8(2)	A	3*T*, (?)	3*T* part, scarce weak reflections of unknown polytype
NB28	5.5146(15)	9.549(2)	7.355(2)	90	375.02(18)	A	1*M*, (3*T*)	1*M* part, twinned by 120° rotation, selected for EPMA
NB30	5.5071(12)	9.5489(19)	7.3526(16)	104.49(2)	374.36(14)	A	1*M*	Twinned by 120° rotation
NB31	5.5126(14)	9.541(2)	7.354(2)	104.63(3)	374.22(16)	A	1*M*	Selected for EPMA
NB32	5.5066(7)		21.313(3)	90	559.69(13)	A	3*T*	pure 3*T*
NB33	5.5066(10)		21.296(4)	90	559.23(19)	A	3*T*, (1*M*)	3*T* part

Space groups of polytypes: 3*T*: $P3_1$, 1*M*: *Cm*

Technologies, Santa Clara, California) at the Institute of Physics, Academy of Sciences, Prague. The MoKα radiation, with graphite monochromator, λ = 0.71070 Å, and a Mo-enhanced fiber-optic collimator were used throughout all experiments.

A pre-experiment was performed first, in order to set parameters for the full experiment. Then a quick full experiment with some parameters reduced (mainly exposure time) was started. Typically, ~450–500 frames were recorded. The total experiment time varied from 10 to 100 min. The *CrysAlisPro*, version 171.40.35a (Rigaku Oxford Diffraction 2018), package was used for the data collection, lattice-parameter calculations, and data processing. The 'unwarp' procedure created user-defined images of reciprocal space sections (henceforth referred to as RS sections) – the equivalents of precession photographs. In some cases the full experiment was repeated with modified parameters, mainly longer exposures, in order to obtain more precise data as well as smoother and less noisy RS sections appropriate for publication.

The RS sections corresponding to six important reciprocal lattice planes were generated: $(2h\bar{h}l_{hex})$*, (hhl_{hex})*, $(\bar{h}2hl_{hex})$*, $(h0l_{hex})$*, $(0kl_{hex})$*, and $(\bar{h}hl_{hex})$*. In the orthohexagonal setting, valid also for monoclinic polytypes, these planes are denoted as follows: $(h\bar{3}hl_{ort,\ mon})$*, $(h0l_{ort,\ mon})$*, $(h3hl_{ort,\ mon})$*, and $(h\bar{h}l_{ort,\ mon})$*, $(hhl_{ort,\ mon})$*, $(0kl_{ort,\ mon})$*. Distributions of

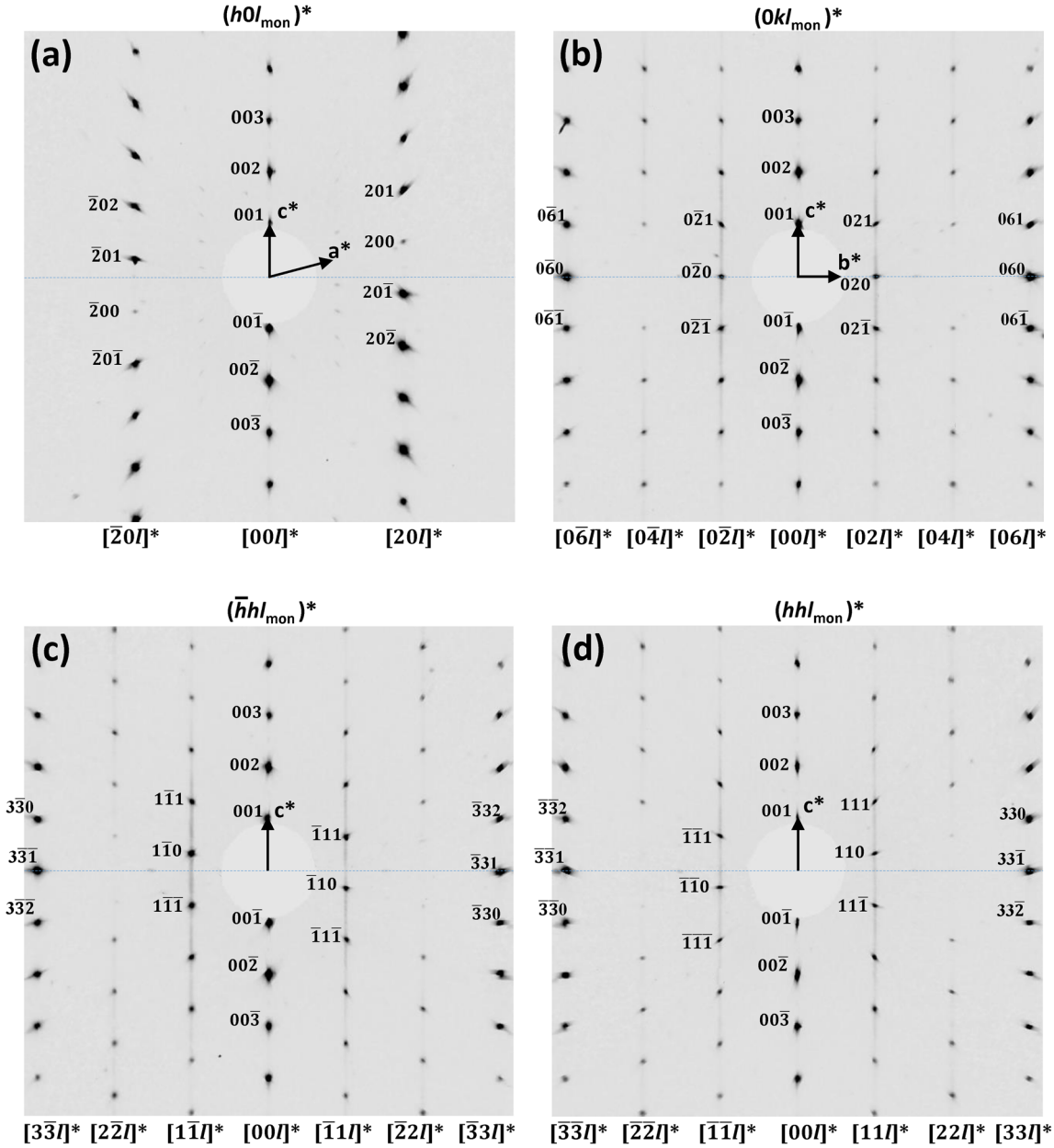

Fig. 2. RS sections of the 1*M* polytype of cronstedtite from Nagybörzsöny. Indices of reciprocal lattice rows and of selected reflections, as well as reciprocal lattice vectors, are indicated. Auxiliary dotted horizontal lines passing through origins of sections are added to aid the eye. **a** The ($h0l_{mon}$)* RS section contains the subfamily reflections characteristic of the A group indexed with respect to the monoclinic cell of the polytype. **b** The ($0kl_{mon}$)* section perpendicular to the *m* plane of the monoclinic unit cell. Note the single periodicity of rows of characteristic reflections at the same levels as reflections of the [00*l*]* row. **c**, **d** The ($\bar{h}hl_{mon}$) (mirror image of ($h\bar{h}l_{mon}$)), and (hhl_{mon})* sections, diagonal to the *m* plane. The rows of characteristic reflections [1$\bar{1}l$]*, [$\bar{1}$1*l*]*, [$\bar{1}$ $\bar{1}l$]*, and [11*l*]* are also single periodic, but shifted by 1/3 **c*** or –1/3 **c*** with respect to [00*l*]* reflections

subfamily reflections along the reciprocal lattice rows [2$\bar{1}l$]* / [11*l*]* / [$\bar{1}$2*l*]* in ($2h\bar{h}l_{hex}$)* / (hhl_{hex})* / ($\bar{h}2hl_{hex}$)* RS sections (i.e. [1$\bar{3}l$]* / [10*l*]* / [13*l*]* in ($h\bar{3}hl_{mon}$)*/ ($h0l_{mon}$)*/ ($h3hl_{mon,}$)* RS sections in the monoclinic setting), were used to determine OD subfamilies (Bailey's groups) A, B, C, D (Dornberger-Schiff and Ďurovič 1975a, b; Bailey 1969, 1988). Similarly, distributions of characteristic reflections along [10*l*]* / [01*l*]* / [$\bar{1}$1*l*]* rows in ($h0l_{hex}$)* / ($0kl_{hex}$)* / ($\bar{h}hl_{hex}$) RS sections (i.e. [1$\bar{1}l$]* / [11*l*]* / [02*l*]* in ($h\bar{h}l_{mon}$)*/ (hhl_{mon})*/ ($0kl_{mon,}$)* in the monoclinic setting) allowed determination of particular polytypes. For this purpose, graphical identification diagrams simulating distribution of reflections along named rows

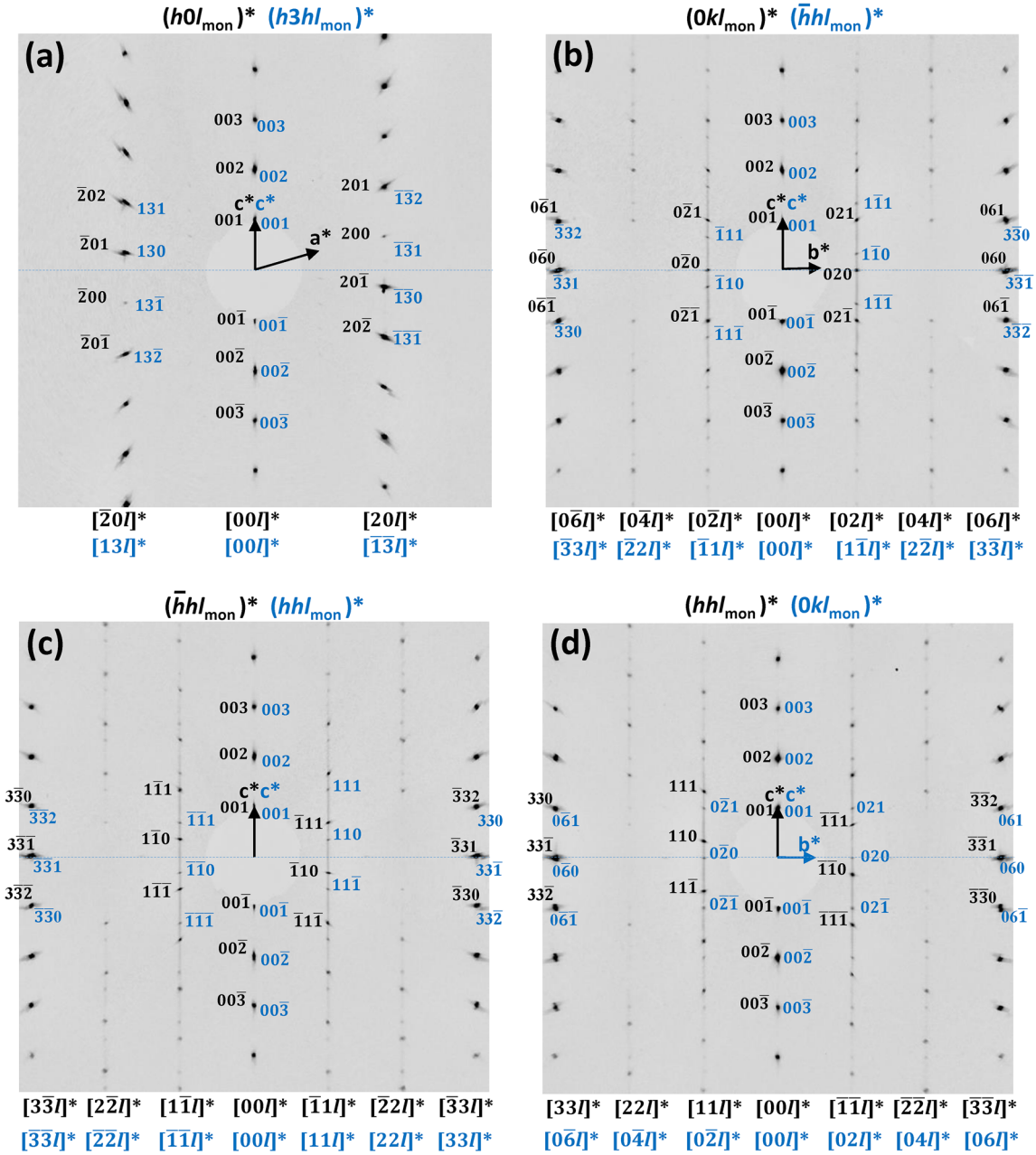

Fig. 3. RS sections of the crystal of the 1*M* polytype of cronstedtite twinned by reticular merohedry, with +120° along $\mathbf{c}_{hex}$ rotation as a twin operation. Indices of rows and reflections of the first (stronger) and second (weaker) twin individuals are shown in black and blue, respectively. **a** The ($h0l_{mon}$)* RS plane corresponding to the ($h3hl_{mon}$)* of the second twin individual. **b** The ($0kl_{mon}$)* section perpendicular to the *m* plane of the first twin individual superimposed on the ($\bar{h}hl_{mon}$)* diagonal section of the second twin individual. **c** Superimposed diagonal ($\bar{h}hl_{mon}$)* and (hhl_{mon})* sections of the first and second twin individuals, respectively. **d** The diagonal (hhl_{mon})* section of the first twin individual superimposed on the perpendicular ($0kl_{mon}$)* section of the second twin individual

were used (Hybler et al. 2018). The lattice parameters of polytypes were calculated using the *CrysAlisPro* software.

A more detailed description of the interpretation of RS sections can be found in recent studies by Hybler et al. (2016, 2018). The lattice parameters of the crystals studied are presented in Table 1.

Electron Probe Microanalysis

The selected fragments of cronstedtite crystals (14 altogether), in which polytypes were determined, were mounted on epoxy discs, polished by diamond suspensions, and coated with a carbon layer ~30 nm thick. The polished grains were analyzed at the National Museum in Prague using a CAMECA

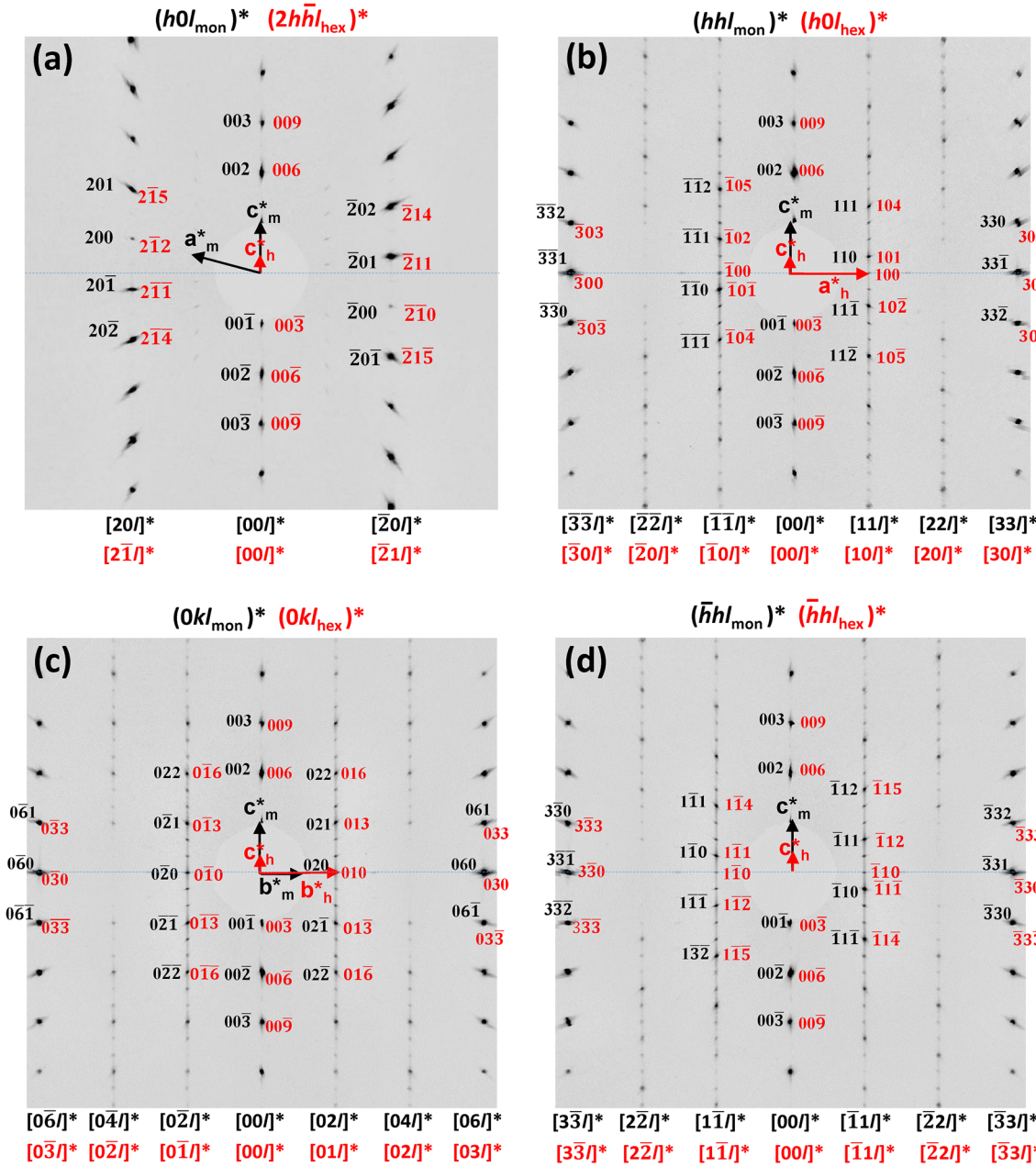

Fig. 4. RS sections of the mixed crystal of 1*M* and 3*T* polytypes. Reciprocal lattice vectors, indices of rows and selected reflections of 1*M* and 3*T* polytypes are shown in black and red, respectively. **a** The $(h0l_{mon})^*$ RS section of 1*M* corresponds to the $(2h\bar{h}l_{hex})^*$ section of the 3*T* polytype. The indexing of the 3*T* polytype (hexagonal indices) is optional, six possible unit cell choices exist. **b** The diagonal $(hhl_{mon})^*$ RS section of 1*M* and $(h0l_{hex})^*$ section of 3*T* polytypes superimposed. **c** The perpendicular $(0kl_{mon})^*$ section of 1*M* and $(0kl_{hex})^*$ section of 3*T* polytypes superimposed. **d** The second diagonal $(\bar{h}hl_{mon})^*$ section of 1*M* and $(\bar{h}hl_{hex})^*$ section of 3*T* polytypes superimposed

SX-100 electron probe micro analyzer (CAMECA, Gennevilliers Cedex, France) operating in wave-dispersive (WDS) mode with acceleration voltage of 15 kV, beam current of 10 nA, and beam diameter of 5 μm. The following standards and analytical lines were used: albite (NaKα), fluorapatite (PKα), celestite (SKα), diopside (MgKα), halite (ClKα), chalcopyrite (CuKα), LiF (FKα), rhodonite (MnKα), sanidine (KKα, SiKα, AlKα), wollastonite (CaKα), and ZnO (ZnKα). The peak counting times were between 10 and 20 s and a half of the peak time was used for both background positions. The raw counts were converted to wt.% using the standard PAP procedure (Pouchou and Pichoir 1985). Oxygen was calculated from the stoichiometry. Elements from the list above which do not appear in the tables, in all cases, occurred at levels

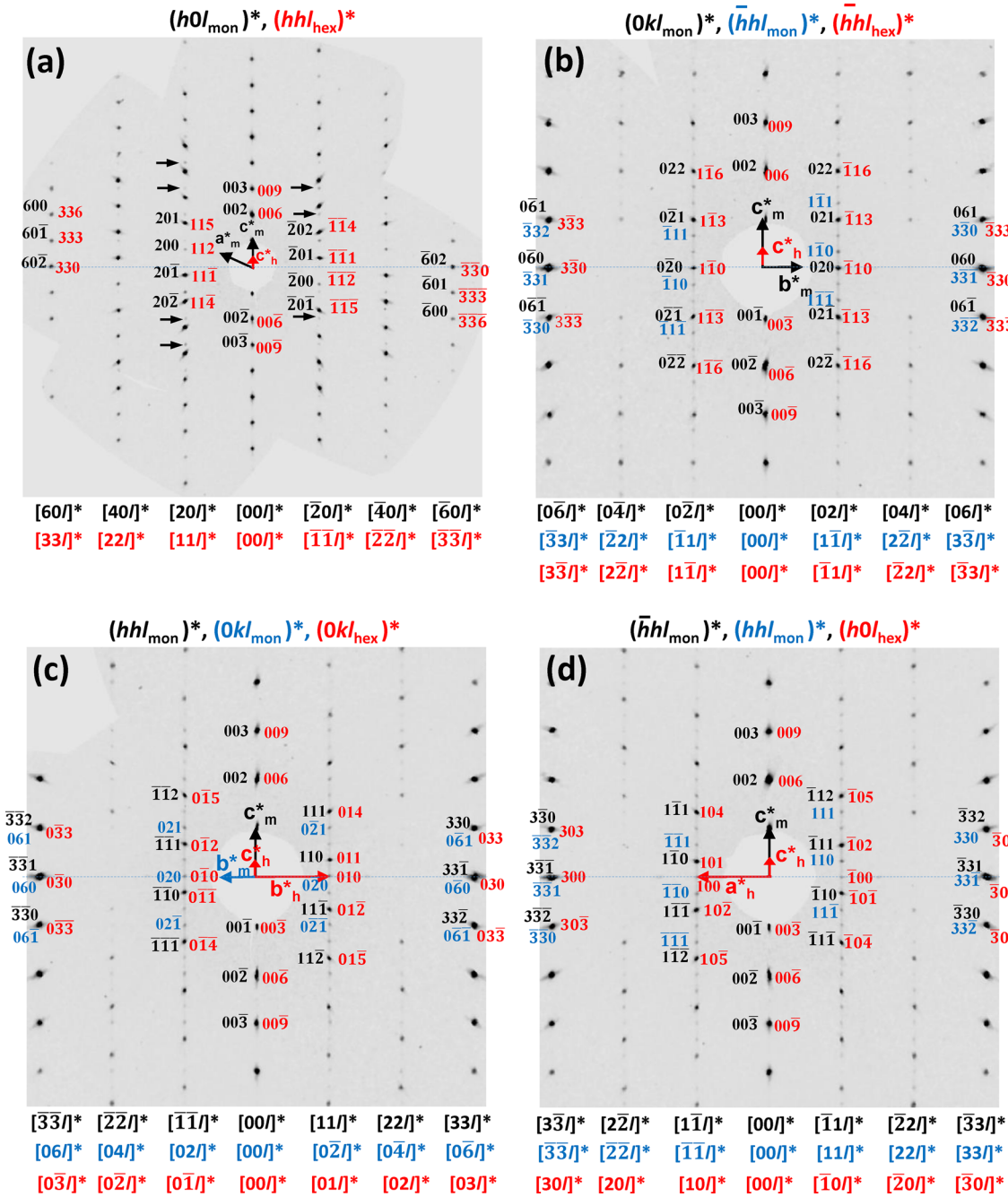

Fig. 5. RS sections of the 1*M*+3*T* mixed crystal, with the 1*M* part twinned by 120° rotation along $\mathbf{c}_{hex}$. In addition, weak, extra reflections belonging to subfamily C are present. Indices of rows and reflections of the first (stronger) and second (weaker) individuals are shown in black and blue, respectively, and those of the 3*T* polytype are in red. The reciprocal unit-cell vectors in respective colors are indicated when possible. The $\mathbf{c}^*_m$ vectors of both twin individuals are identical. **a** Superimposed $(h0l_{mon})^*$ and $(hhl_{hex})^*$ RS sections, with some of the subfamily C reflections (not indexed) indicated by arrows. These reflections are at the same levels as the [00*l*]* ones. For the sake of clarity, the indices of the weaker individual of the 1*M* polytype were omitted. This RS section is presented at a scale which is different ('zoomed out') from other sections in order to present a larger proportion of the reciprocal space. **b** The perpendicular $(0kl_{mon})^*$ section of the stronger + diagonal $(\bar{h}hl_{mon})^*$ section of the weaker individuals of the 1*M* + $(\bar{h}hl_{hex})^*$ section of the 3*T* superimposed. **c** Superposition of the diagonal $(hhl_{mon})^*$ section of the stronger individual + perpendicular $(0kl_{mon})^*$ section of the weaker individual of the 1*M* + $(0kl_{hex})^*$ section of the 3*T* polytypes. **d** Superposition of two diagonal sections of $(\bar{h}hl_{mon})^*$ and $(hhl_{mon})^*$ of the strong and weak individuals of the 1*M*, respectively, + $(h0l_{hex})^*$ section of the 3*T* polytype

which were below the limits of detection. The amounts of H_2O, Fe^{2+}, and Fe^{3+} as well as *x*-values were calculated on the basis of the general formula of cronstedtite $(Fe^{2+}_{3-x}Fe^{3+}_{x})(Si_{2-x}Fe^{3+}_{x})O_5(OH)_4$.

RESULTS AND DISCUSSION

With one exception, discussed below, all polytypes identified in the crystals studied belong entirely to subfamily A (Bailey's group). The stacking rule of this group is represented by the ensemble of $\pm\mathbf{a}_i/3$ shifts of consecutive 1:1 layers (without any rotation).

The most remarkable finding in the present study was the relative abundance of the otherwise rare 1*M* polytype, lattice parameters a = 5.51, b = 9.54, c = 7.33 Å, β = 104.5°, space group *Cm*. This polytype is quite common in the occurrence and provides well developed crystals. The RS sections of one of the crystals studied are presented in Fig. 2. The $(h0l_{mon})$* RS section corresponds to one of three (identical) $(2h\bar{h}l_{hex})$* / (hhl_{hex})* / $(\bar{h}2hl_{hex})$* (i.e. $(\bar{h}3hl_{mon})$* / $(h0l_{mon})$* / $(h3hl_{mon})$*) planes containing the subfamily reflections in the arrangement characteristic of the A subfamily (Fig. 2a). Reflections in [20*l*]* and [$\bar{2}$0*l*]* rows were shifted vertically by –1/3 and 1/3, respectively, of the periodicity of the [00*l*]* row, in accordance with the graphical identification diagram by Hybler et al. (2018), for example. Reciprocal lattice rows and selected reflections were indexed according to the polytype and reciprocal lattice vectors are indicated. This section corresponds to the *m* plane of the polytype in direct space.

The following $(h0l_{hex})$* / $(0kl_{hex})$* / $(\bar{h}hl_{hex})$* RS sections ($(h\bar{h}l_{mon})$* / (hhl_{mon})* / $(0kl_{mon})$* in monoclinic indexing) were unequal due to the monoclinic character of the polytype. The $(0kl_{mon})$* section (Fig. 2b) was perpendicular to the *m* plane. The characteristic reflections in rows [02*l*]* and [0$\bar{2}$*l*]* reflected the single periodicity. Two remaining sections $(h\bar{h}l_{mon})$* and (hhl_{mon})* were diagonal to the *m* plane. The rows of characteristic reflections [1$\bar{1}$*l*]*, [$\bar{1}$1*l*]*, [$\bar{1}$ $\bar{1}$*l*]*, and [11*l*]* were also single periodic, but shifted by 1/3 **c*** or –1/3 **c*** with respect to [00*l*]* reflections (Fig. 2c,d).

The 'pure' 1*M* polytype is rare in terrestrial samples. A unique crystal from Lutherstadt Eisleben, Germany, was studied by Hybler (2014), who performed a structure refinement and presented RS sections. On the other hand, the pure 1*M* polytype was found to be relatively abundant in the synthetic run product quoted by Pignatelli et al. (2013, 2020) and Hybler et al. (2018).

The 1*M* polytype is often affected by twinning by order 3 reticular merohedry, with +120° or –120° rotation along $\mathbf{c}_{hex}$ as the twinning operation. Several twinned crystals were found in the Nagybörzsöny samples, and RS sections of one of them are presented in Fig. 3. Two sections represent superposition of one perpendicular and one diagonal section of two individuals (Fig. 3b,d), while the third section represents superposition of two diagonal sections arranged as mutual mirror images (Fig. 3c). The amounts of particular twin individuals in the crystal are unequal, so that the respective subsets of reflections are unequally intense. The $(h0l_{mon})$* RS section containing entirely so-called subfamily reflections common for all polytypes of the A subfamily is not affected by this kind of twinning. However, two alternative indices are possible, either $(h0l_{mon})$* or $(h3hl_{mon})$*, according to the first and second twin individual, respectively (Fig. 3a).

Another A group polytype present in the Nagybörzsöny occurrence is 3*T*, lattice parameters a = 5.51, c = 21.32 Å, space group $P3_1$ or $P3_2$. This polytype is quite common (the most frequent of all A group polytypes), and it has been referred from many localities recently e.g. from Příbram, Chvaletice, Pohled, and Nižná Slaná (Smrčok et al. 1994;

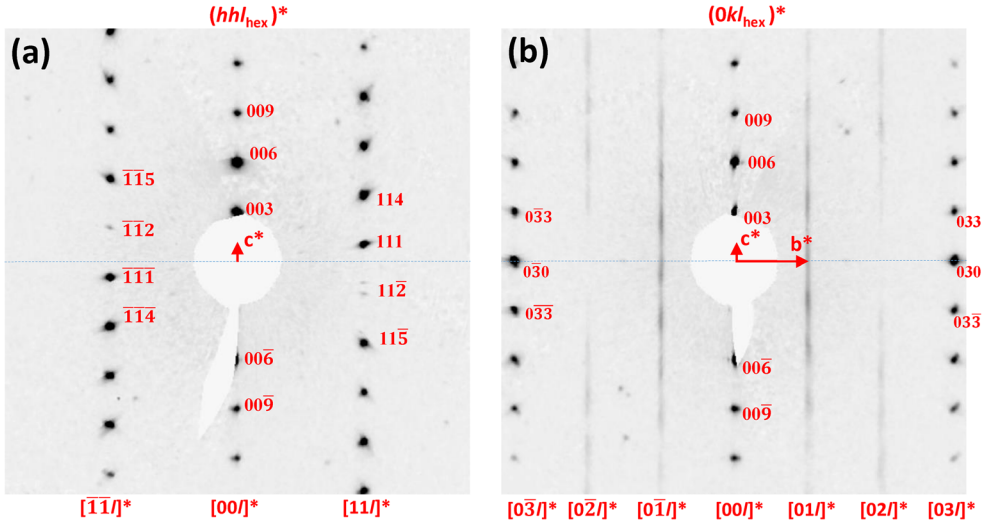

Fig. 6. RS section of the disordered crystal of the subfamily A. Reciprocal lattice rows and reflections are indexed with respect to the 3*T* polytype. **a** The subfamily reflections in the (hhl_{hex})* RS section are not affected by the stacking disorder. **b** In the $(0kl_{hex})$* RS section the rows of characteristic reflections ([01*l*]*, [02*l*]*, [0$\bar{1}$*l*]* and [0$\bar{2}$*l*]*) are replaced by diffuse streaks. An unequal density along streaks indicates a certain low degree of ordering, however. The [03*l*]* and [0$\bar{3}$*l*]* rows contain sharp subfamily reflections

Table 2. Chemical compositions (wt.%) of the cronstedtite crystals from Nagybörzsöny and calculated a.p.f.u. values

Polytype	disordered	disordered	disordered	disordered	1*M*	1*M*	1*M*	1*M* (+3*T*)	1*M* (+3*T*)	1M (+3*T*)	3*T* (+1*M*)	3*T* (+1*M*)	3*T* (+1*M*)	3*T* (+1*M*)
Sample	NB11	NB11	NB10	NB11	NB31	NB31	NB31	NB28	NB28	NB28	NB1	NB19	NB1	NB19
SiO_2	17.33	17.90	18.07	18.80	17.32	17.88	18.19	17.80	17.74	18.24	17.57	17.94	18.05	18.70
Al_2O_3	0.09	0	0	0	0	0	0	0	0	0	0	0	0	0
Fe_2O_3	33.77	33.02	31.58	31.07	33.53	32.76	30.93	32.95	32.11	31.44	33.74	32.50	32.23	31.12
FeO	38.72	39.54	39.51	40.48	38.61	39.28	39.44	39.34	39.04	39.79	39.11	39.49	39.63	40.54
MgO	0	0	0	0.13	0	0.09	0.08	0	0	0	0	0	0	0
S	0.06	0.05	0.08	0.05	0.06	0.04	0.04	0.04	0.06	0.06	0.06	0.05	0.04	0.05
H_2O	9.01	9.08	8.96	9.13	8.96	9.05	8.93	9.04	8.92	9.00	9.06	9.03	9.04	9.10
Total	98.97	99.59	98.19	99.67	98.48	99.10	97.61	99.18	97.87	98.54	99.54	99.02	98.99	99.52
Si^{4+}	1.152	1.181	1.206	1.233	1.157	1.184	1.220	1.179	1.190	1.213	1.161	1.189	1.196	1.230
Al^{3+}	0.007	0	0	0	0	0	0	0	0	0	0	0	0	0
Fe^{3+}	1.689	1.639	1.587	1.534	1.686	1.632	1.561	1.642	1.621	1.573	1.678	1.621	1.607	1.540
Fe^{2+}	2.152	2.181	2.206	2.220	2.157	2.175	2.212	2.179	2.190	2.213	2.161	2.189	2.196	2.230
Mg^{2+}	0	0	0	0.013	0	0.009	0.008	0	0	0	0	0	0	0
ΣCat	5	5	5	5	5	5	5	5	5	5	5	5	5	5
S	0.007	0.006	0.010	0.006	0.008	0.005	0.005	0.005	0.008	0.008	0.007	0.006	0.004	0.006
OH	3.993	3.994	3.990	3.994	3.992	3.995	3.995	3.995	3.992	3.992	3.993	3.994	3.996	3.994
ΣAn	4	4	4	4	4	4	4	4	4	4	4	4	4	4
X	0.85	0.82	0.79	0.77	0.84	0.82	0.78	0.82	0.81	0.79	0.84	0.81	0.80	0.77

The H_2O content (4 OH+S p.f.u.), Fe^{3+}/Fe^{2+} ratio, and *x* value were calculated based on the stoichiometry of general formula $(Fe^{2+}_{3-x}Fe^{3+}_{x})(Si_{2-x}Fe^{3+}_{x})O_5(OH)_4$

Table 3. Variations in chemical composition of the studied polytypes of cronstedtites from Nagybörzsöny. Contents of ions per formula unit are given

Polytype	Samples	*n*		Si	Al	Fe^{3+}	Fe^{2+}	Mg	S	Cl	OH	*X*
disordered	NB10, NB11	16	average	1.199	0.000	1.602	2.196	0.003	0.007	0.001	3.993	0.80
			minimum	1.164	0.000	1.534	2.152	0.000	0.005	0.000	3.984	0.77
			maximum	1.233	0.007	1.689	2.232	0.013	0.010	0.009	3.995	0.85
1*M*	NB31	8	average	1.189	0.001	1.621	2.187	0.002	0.006	0.000	3.994	0.81
			minimum	1.157	0.000	1.561	2.157	0.000	0.004	0.000	3.992	0.78
			maximum	1.220	0.006	1.686	2.217	0.009	0.008	0.000	3.996	0.84
1*M* (+3*T*)	NB28	7	average	1.200	0.000	1.599	2.198	0.002	0.007	0.000	3.993	0.80
			minimum	1.179	0.000	1.573	2.179	0.000	0.005	0.000	3.991	0.79
			maximum	1.213	0.000	1.642	2.213	0.016	0.009	0.000	3.995	0.82
3*T* (+1*M*)	NB1, NB19	16	average	1.193	0.001	1.613	2.192	0.001	0.006	0.000	3.994	0.81
			minimum	1.161	0.000	1.540	2.161	0.000	0.004	0.000	3.992	0.77
			maximum	1.230	0.007	1.678	2.230	0.008	0.008	0.000	3.996	0.84

n – number of spot analyses

Hybler 1998; Hybler et al. 2016, 2017). The 3*T* polytype occurs either isolated, or in mixed crystals with the 1*M* polytype. The diffraction pattern is a superposition of a triply periodic pattern of 3*T* and of monoclinic 1*M* described above (Fig. 4). As a result, every third diffraction spot in $[10l]^*$ / $[01l]^*$ / $[\bar{1}1l]^*$ rows (hexagonal indexing) is stronger than its neighbors. In the section perpendicular to the mirror plane of 1*M*, the $l = 3n$ reflections of 3*T* are stronger (Fig. 4c). In the other two sections the $l = 3n + 1$ or $l = 3n + 2$ reflections are stronger (Fig. 4b,d). The $(h0l_{mon})^*$ RS section corresponds to $(2h\bar{h}l_{hex})^*$ plane of 3*T* (Fig. 4a).

Such mixed crystals are known from other localities (e. g. Pohled). This phenomenon was studied and modeled by Ďurovič (1997) for the various proportions of both polytypes. The 3*T*+1*M* mixed crystals were observed in reality by Steadman and Nuttall (1964), and also mentioned by Bailey (1988). However, in most such mixed crystals, the 3*T* polytype is usually dominant and differences in intensities are not significant. In the Nagybörzsöny cronstedtite, dominant 1*M* crystals were found, with superimposed 3*T*+1*M* reflections noticeably stronger than mere 3*T* reflections (Fig. 4).

Among the crystals studied, one rare complex crystal containing 1*M*+3*T* polytypes with the 1*M* part twinned by 120° rotation (Fig. 5) was found. The 1*M* part consisted of 'stronger' and 'weaker' twin individuals (cf. Figs 3 and 5). Their diffraction patterns were superimposed on those of the 3*T* polytype. Moreover, the $(2h\bar{h}l_{hex})^*$/ $(hhl_{hex})^*$/ $(\bar{h}2hl_{hex})^*$ RS sections contained weak extra reflections in the arrangement corresponding to the subfamily C, placed at the same level as the $[00l]^*$ reflections. It is thus a complex mixed crystal of A+C subfamilies, the only one in the occurrence. The presence of the most common polytype 1*T* of the C subfamily remains uncertain, because its characteristic reflections are arranged identically with characteristic reflections of the perpendicular sections of the 1*M* polytype. They are thus overlapped by $l = 3n$ reflections of the 3*T* polytype, and, of course, of 1*M* reflections in perpendicular sections. Note also that the recorded subfamily C reflections are weaker and smaller than the subfamily A ones (see Fig. 5a). They were probably produced by a limited area within the crystal composed mainly of subfamily A polytypes.

Mixed crystals of subfamilies A+C are rare. The C subfamily reflections were recognized in RS sections recorded by EDT of several crystals of the 1*M* polytype from the synthetic run product (Hybler et al. 2018). In most cases no ordered C subfamily polytype was found, however, with the exception of one mixed 1*M*+1*T* crystal. Here, because of absence of the 3*T* polytype, the 1*T* polytype was easily distinguished. The electron diffraction pattern of 1*M*+1*T* (A+C) mixed crystal of meteoritic cronstedtite from the Cochabamba carbonaceous chondrite was published by Müller et al. (1979).

Several crystals in the occurrence are completely or almost completely disordered. In the diffraction pattern, the so-called subfamily reflections – common for all polytypes of the A subfamily (Bailey's group) – remain sharp, while the rows of characteristic reflections are replaced by diffuse streaks. A good example of RS sections of such a crystal is presented in Fig. 6. The indices of reflections and rows are related to the unit cell of the so-called subfamily structure, a fictitious structure resulting from superposition of all possible shifts of the OD packet (i.e. structure building 1:1 layer) allowed by the stacking rule of the subfamily A; the unit cell corresponds formally to that of the 3*T* polytype.

Note that diffraction patterns of other crystals also contain diffusion strips along the rows of characteristic reflections (Figs 2–5). The reflections themselves remain sharp, however.

CHEMICAL COMPOSITION

The chemical composition (Table 2) revealed no systematic differences between individual polytypes. The BSE imaging

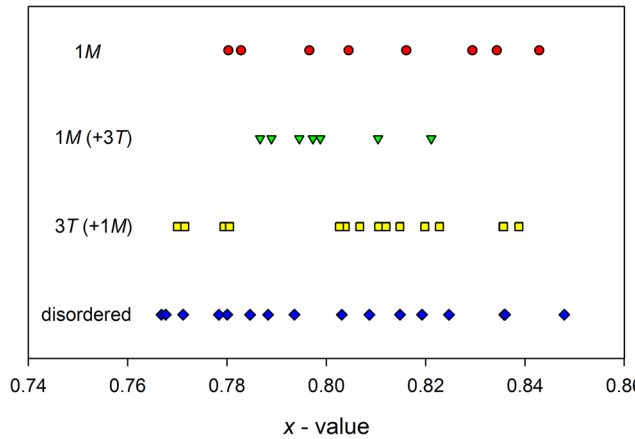

Fig. 7. Range of calculated *x* for individual cronstedtite polytypes

suggested that all the fragments of cronstedtite crystals were compositionally homogeneous. In order to examine compositional variability, 47 spot analyses were collected from six selected samples (Table 3). The data revealed a simple composition of all the cronstedtite samples studied, with negligible minor elements contents. The Si contents ranged between 1.157 and 1.233 a.p.f.u., Fe^{3+} between 1.534 and 1.689 a.p.f.u., and Fe^{2+} between 2.152 and 2.232 a.p.f.u.. The *x*-values in the general formula ranged between 0.77 and 0.85. The ranges of calculated *x* value for individual polytypes were comparable (Fig. 7). All compositions showed low levels of S (0.004–0.010 a.p.f.u. of S substituting for OH); these amounts did not correlate with the polytype determined or the *x* value calculated (Fig. 8). Detectable levels of other elements were recorded only exceptionally (Al ≤ 0.007 a.p.f.u., Mg ≤ 0.016 a.p.f.u., Cl ≤ 0.009 a.p.f.u.). No traces of Mn were detected.

ACCOMPANYING PHASES

One black fragment selected from the ore material originally considered to be cronstedtite provided different hexagonal lattice parameters a = 3.8306(5), c = 9.3844(14) Å. These parameters matched those of alleged 3*R* polytype of ZnS structure, known as 'matraite,' described from Gyöngyösoroszi, Mátra mountains, Hungary (Koch 1958; Sasvári 1958). This mineral was later discredited (Niita et al. 2008), however, and found to be identical to (111) multiply twinned sphalerite. The indexation of diffraction data using a twin option in *CrysAlis* clearly confirmed a cubic cell with a = 5.4171(4) Å, in a good agreement with sphalerite (e.g. Becker and Lutz 1978). The $(\overline{h}hl_{hex})$* RS section (Fig. 9) revealed twinning which was identical to the scheme in Fig. 2 of Niita et al. (2008). Because the *F*-centered cubic cell of sphalerite can be regarded as a special case of the rhombohedral cell, this twinning can be interpreted as a special case of the so-called 'obverse-reverse' twinning. A quick analysis by EPMA in energy-dispersive (EDS) mode revealed the presence of Zn, S, a small amount of Fe, and traces of Cu. The black crystals of sphalerite might sometimes be mistaken for cronstedtite, especially if they are developed in columnar or acicular form due to multiple twinning. Their mechanical properties are different, however; sphalerite is harder and cannot be cleaved easily into thin plates.

Several honey-brown crystals grown on the cronstedtite substrate or thin crusts of siderite partially covering cronstedtite crystals were observed. Some cronstedtite crystals were partially replaced by siderite pseudomorphs close to one end. Two fragments of siderite were separated and tested using single-crystal

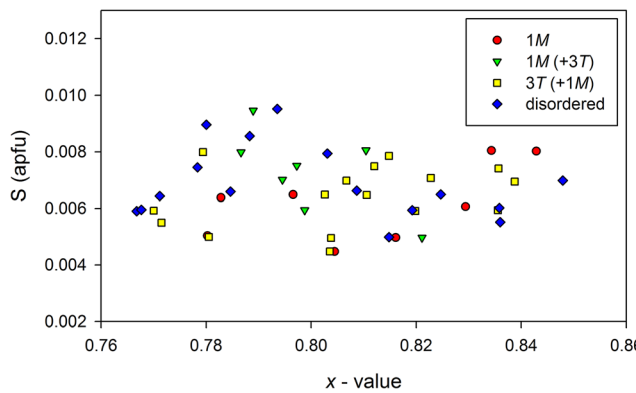

Fig. 8. Graph of calculated *x* vs S contents (a.p.f.u.) for individual cronstedtite polytypes

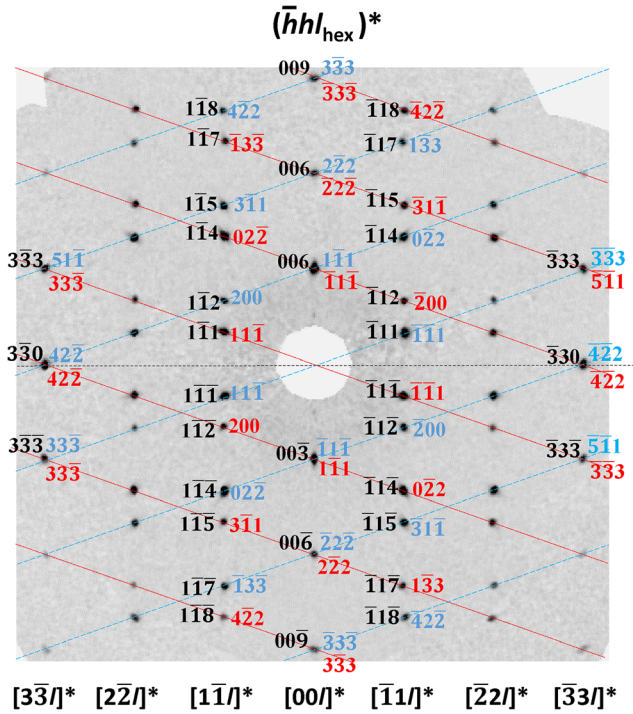

Fig. 9. RS section $(\bar{h}\bar{h}l_{hex})^*$ of the multiple twin of sphalerite. Hexagonal indices of selected reflections related to the "mátraite" pseudocell are in black; cubic indices related to the first and second twin individuals are in blue and red, respectively. Reflections belonging to respective twin individuals are connected by blue and red auxiliary lines. In the [3$\bar{3}$*l*]*, [00*l*]*, and [$\bar{3}$3*l*]* rows the reflections of both twin individuals are overlapped; in the remaining ones, they are separated

diffractometry. The lattice parameters were a = 4.6910(15), c = 15.371(6) Å, in good agreement with those for siderite (Effenberger et al. 1981). The EPMA in EDS mode revealed Fe, C, O, and traces of Mg, Al, Ca, and S. Siderite together with pyrite constitute the majority of the ore material.

CONCLUSIONS

Cronstedtite from the Nagybörzsöny occurrence has interesting properties: (1) well developed crystals of the rare polytype 1*M*; (2) twinning by reticular merohedry by 120° rotation along $\mathbf{c}_{hex}$ of the 1*M* polytype; (3) mixed crystals of 1*M*+3*T* polytypes with the 1*M* polytype significantly dominant; (4) the 1*M* and 3*T* polytypes identified in the sample belong to standard polytypes – they are also known as MDO (Maximum Degree of Order) polytypes, in which all layer triples, quadruples, etc. are equivalent; (5) copybook examples of disordered crystals of the A group were found; (6) cronstedtite crystals in the sample studied occurred isolated, not in aggregates – veins or druses; a possible sample with aggregates was mentioned by Koch and Graselly (1953) but none of the material from their study was available for study; (7) all EPMA analyses reveal pure cronstedtite with very minor substitutions for Fe; as in the previous studies, no significant differences in composition of particular polytypes or disordered crystals were observed.

ACKNOWLEDGMENTS

The authors thank collector Gábor Koller for providing the sample. M. Jarošová checked the compositions of accompanying phases. L. Jilemnická read the manuscript critically. Valuable comments by two anonymous referees are appreciated. The study was supported by project No. LO1603 under the Ministry of Education, Youth and Sports National sustainability programme 1 of Czech Republic to JH, and by institutional funding of the National Museum as a research organization 00023272 under project DKRVO 2019-2023/1.II.b to ZD and JS.

Funding

Funding sources are as stated in the Acknowledgments.

Compliance with Ethical Statements

Conflict of Interest

The authors declare that they have no conflict of interest.

REFERENCES

Bailey, S. W. (1969). Polytypism of trioctahedral 1:1 layer silicates. *Clays and Clay Minerals, 17*, 355–371. https://doi.org/10.1346/CCMN.1969.0170605.

Bailey, S.W. (1988). Polytypism of 1:1 layer silicates. Pp. 1–27 in: *Hydrous Phyllosilicates (Exclusive of micas)* (S.W. Bailey, editor). Reviews in Mineralogy, *19*, Mineralogical Society of America, Washington, D.C.

Becker, W., & Lutz, H. D. (1978). Phase studies in the systems CoS-MnS, CoS-ZnS, and CoS-CdS. *Materials Research Bulletin, 13*, 907–911. https://doi.org/10.1016/0025-5408(78)90102-2.

Bindi, L., & Paar, W. H. (2017). Jaszczakite, $[(Bi, Pb)_3S_3][AuS_2]$, a new mineral species from Nagybörzsöny. *Hungary. European Journal of Mineralogy, 29*(4), 673–677. https://doi.org/10.1127/ejm/2017/0029-2620.

Dobosi, G., & Nagy, B. (1989). The occurrence of an Au-Bi sulphide in the Nagybörzsöny hydrothermal ore deposit, northern Hungary. *Neues Jahrbuch für Mineralogie Monatshefte*, 8–14.

Dornberger-Schiff, K., & Ďurovič, S. (1975a). OD-interpretation of kaolinite-type structures - I: Symmetry of kaolinite packets and their stacking possibilities. *Clays and Clay Minerals, 23*, 219–229. https://doi.org/10.1346/CCMN.1975.0230310.

Dornberger-Schiff, K., & Ďurovič, S. (1975b). OD-interpretation of kaolinite-type structures - II: The regular polytypes (MDO-polytypes) and their derivation. *Clays and Clay Minerals, 23*, 231–246. https://doi.org/10.1346/CCMN.1975.0230311.

Ďurovič, S. (1997). Cronstedtite-1*M* and coexistence of 1*M* and 3*T* polytypes. *Ceramics-Silikáty, 41*, 98–104.

Effenberger, H., Mereiter, K., & Zemann, J. (1981). Crystal structure refinements of magnesite, calcite, rhodochrosite, siderite, smithonite, and dolomite, with the discussion of some aspects of the stereochemistry of calcite type carbonates. *Zeitschrift für Kristallographie, 156*, 233–243. https://doi.org/10.1524/zkri.1981.156.3-4.233.

Geiger, C. A., Henry, D. L., Bailey, S. W., & Maj, J. J. (1983). Crystal structure of cronstedtite-$2H_2$. *Clays and Clay Minerals, 31*, 97–108. https://doi.org/10.1346/CCMN.1983.0310203.

Hybler, J. (1998). Polytypism of cronstedtite from Chvaletice and Litošice. *Ceramics-Silikáty, 42*, 130–131.

Hybler, J. (2014). Refinement of cronstedtite-1*M*. *Acta Crystallographica, B70*, 963–972. https://doi.org/10.1107/S2052520614020897.

Hybler, J. (2016). Crystal structure of cronstedtite-$6T_2$, a non-MDO polytype. *European Journal of Mineralogy, 28*, 777–788. https://doi.org/10.1127/ejm/2016/0028-2541.

Hybler, J., Klementová, M., Jarošová, M., Pignatelli, I., Mosser-Ruck, R., & Ďurovič, S. (2018). Polytypes identification in trioctahedral layer silicates by electron diffraction and application to cronstedtite mineral synthetized by iron-clay interaction. *Clays and Clay Minerals, 66*, 379–402. https://doi.org/10.1346/CCMN.2018.064106.

Hybler, J., Petříček, V., Ďurovič, S., & Smrčok, L. (2000). Refinement of the crystal structure of cronstedtite-1*T*. *Clays and Clay Minerals, 48*, 331–338. https://doi.org/10.1346/CCMN.2000.0480304.

Hybler, J., Petříček, V., Fábry, J., & Ďurovič, S. (2002). Refinement of the crystal structure of cronstedtite-$2H_2$. *Clays and Clay Minerals, 50*, 601–613. https://doi.org/10.1346/000986002320679332.

Hybler, J., & Sejkora, J. (2017). Polytypism of cronstedtite from Chyňava, Czech Republic. *Journal of Geosciences, 62*, 137–146. https://doi.org/10.3190/jgeosci.239.

Hybler, J., Sejkora, J., & Venclík, V. (2016). Polytypism of cronstedtite from Pohled, Czech Republic. *European Journal of Mineralogy, 28*, 765–775. https://doi.org/10.1127/ejm/2016/0028-2532.

Hybler, J., Števko, M., & Sejkora, J. (2017). Polytypism of cronstedtite from Nižná Slaná, Slovakia. *European Journal of Mineralogy, 29*, 91–99. https://doi.org/10.1127/ejm/2017/0029-2582.

Kenngott, A. (1853). *Das Mohs´sche Mineralsystem*. Wien: Gerold & Sohn 164 pp.

Koch, S. (1958). The associated occurrence of three ZnS modifications in Gyöngyösoroszi. *Acta Universitatis Szegediensis, Acta Mineralogica-Petrographica, 11*, 11–22.

Koch, S., & Grasselly, G. (1953). The minerals of the sulphide ore-deposite of Nagybörzsöny. *Acta Universitatis Szegediensis, Acta Mineralogica-Petrographica, 6*, 1–21.

Kogure, T., Hybler, J., & Ďurovič, S. (2001). A HRTEM study of cronstedtite: determination of polytypes and layer polarity in trioctahedral 1:1 phyllosilicates. *Clays and Clay Minerals, 49*, 310–317. https://doi.org/10.1346/CCMN.2001.0490405.

Kogure, T., Hybler, J., & Yoshida, H. (2002). Coexistence of two polytypic groups in cronstedtite from Lostwithiel, England. *Clays and Clay Minerals, 50*, 504–513. https://doi.org/10.1346/000986002320514226.

Korpás, L., & Lang, B. (1993). Timing of volcanism and metallogenesis in the Börzsöny Mountains, Northern Hungary. *Ore Geology Reviews, 8*, 477–501.

Müller, W. F., Kurat, G., & Kracher, A. (1979). Chemical and crystallographical study of cronstedtite in the matrix of the Cochabamba (*CM*2) carbonaceous chondrite. *Tschermaks Mineralogische und Petrographische Mitteilungen, 26*, 293–304.

Nagy, B. (2002). Data for the mineralogical and geochemical knowledge of the precious metal minerals of the ore deposits and ore indications in the Börzsöny Mts. *Földtani Közlöny, 132*(3–4), 401–421 (In Hungarian with an English abstract).

Niita, E., Kimata, M., Hoshino, M., Echigo, T., Hamasaki, S., Nishida, N., Shimizu, M., & Akasaka, T. (2008). Crystal chemistry of ZnS minerals formed as high-temperature volcanic sublimates: matraite identical with sphalerite. *Journal of Mineralogical and Petrological Sciences, 103*, 145–151. https://doi.org/10.2465/jmps.071022f.

Paar, W. H., Putz, H., Topa, D., Roberts, A. C., Stanley, C. J., & Culetto, F. J. (2006). Jonassonite, $Ag(Bi,Pb)_5S_4$, a new mineral species from Nagybörzsöny, Hungary. *The Canadian Mineralogist, 44*, 1127–1136.

Pantó, G., & Mikó, I. (1964). Nagybörzsöny ore deposit. *Annals of Hungarian Geological Institute, 50*, 1–153 (in Hungarian).

Pignatelli, I., Marrocchi, Y., Mugnaioli, E., Bourdelle, F., & Gounelle, M. (2017). Mineralogical, crystallographic and redox features of the earliest stages of fluid alteration in CM chondrites. *Geochimica et Cosmochimica Acta, 209*, 106–122.

Pignatelli, I., Marrochi, Y., Vacher, L. G., Delon, R., & Gounelle, M. (2016). Multiple precursors of secondary mineralogical assemblages in CM chondrites. *Meteoritic and Planetary Science, 51–4*, 785–805. https://doi.org/10.1111/maps.12625.

Pignatelli, I., Mosser-Ruck, R., Mugnaioli, E., Sterpenich, J., & Gemmi, M. (2020). The effect of the starting mineralogical mixture on the nature of Fe serpentines obtained during hydrothermal syntheses at 90°C. *Clays and Clay Minerals, 68*, 394–412. https://doi.org/10.1007/s42860-020-00080-y.

Pignatelli, I., Mugnaioli, E., Hybler, J., Mosser-Ruck, R., Cathelineau, M., & Michau, N. (2013). A multi-technique characterisation of cronstedtite synthetized by iron-clay interaction in a step by step cooling procedure. *Clays and Clay Minerals, 61*, 277–289. https://doi.org/10.1346/CCMN.2013.0610408.

Pignatelli, I., Mugnaioli, E., & Marrocchi, Y. (2018). Cronstedtite polytypes in the Paris meteorite. *European Journal of Mineralogy*. https://doi.org/10.1127/ejm/2018/0030-2713.

Pouchou, J.L., & Pichoir, F. (1985). "PAP" (φρZ) procedure for improved quantitative microanalysis. Pp. 104–106 in: *Microbeam Analysis* (J.T. Armstrong, editor). San Francisco Press, San Francisco, California, USA.

Rigaku Oxford Diffraction (2018). *CrysAlisPro*, version 171.40.35a, Data collection and data reduction GUI.

Sasvári, K. (1958). ZnS mineral with ZnS-3*R* crystal structure. *Acta Universitatis Szegediensis, Acta Mineralogica-Petrographica, 11*, 23–27.

Smrčok, L., Ďurovič, S., Petříček, V., & Weiss, Z. (1994). Refinement of the crystal structure of cronstedtite-3*T*. *Clays and Clay Minerals, 42*, 544–551. https://doi.org/10.1346/CCMN.1994.0420505.

Steadman, R. (1964). The structure of trioctahedral kaolin-type silicates. *Acta Crystallographica, 17*, 924–927.

Steadman, R., & Nuttall, P. M. (1963). Polymorphism in cronstedtite. *Acta Crystallographica, 16*, 1–8.

Steadman, R., & Nuttall, P. M. (1964). Further polymorphism in cronstedtite. *Acta Crystallographica, 17*, 404–406.

Steinmann, J.J. (1820). Chemische Untersuchung des Cronstedtit's, eines neuen Fossils von Příbram in Böhmen. Gottlieb Haase, Prague, 47 pp. (in German).

Steinmann, J. J. (1821). Chemische Untersuchung des Cronstedtit's, eines neuen Fossils von Příbram in Böhmen. *Journal für Chemie und Physik, 32*, 69–100 (in German).

Szakáll, S., Fehér, B., & Tóth, L. (2016). Hungarian Minerals. GeoLitera, SZTE TTIK, Földrajzi és Földtudományi Intézet, 1–526 (In Hungarian).

Szakáll, S., Zajzon, N., & Kristály, F. (2012). Unusual ikunolite from Nagybörzsöny ore deposit, Börzsöny Mts., Hungary. *Acta Mineralogica-Petrographica, Abstract Series, 7*, 134.

Wahle, M. W., Bujnowski, T. J., Guggenheim, S., & Kogure, T. (2010). Guidottiite, the Mn-analogue of cronstedtite: A new serpentine-group mineral from South Africa. *Clays and Clay Minerals, 58*, 364–376. https://doi.org/10.1346/CCMN.2010.0580307.

Zajzon, N., Szakáll, S., Kristály, F., Hartai, É., & Fehér, B. (2014). Pb-Bi-(Ag)-sulphosalts from Nagybörzsöny, Hungary. *21st Meeting of the International Mineralogical Association,* 136.

(*Received 3 June 2020; revised 24 September 2020; AE: Georgios D. Chryssikos*)